

Emerging orthorhombic two-dimensional van der Waals magnets

Xiaoyu Guo^{1,*}, Wenhao Liu^{2,*}, Bing Lv^{2,*}, Liuyan Zhao^{1,*}

¹ Department of Physics, University of Michigan, Ann Arbor, MI 48019, USA

² Department of Physics, the University of Texas at Dallas, Richardson, TX 75080, USA

* Corresponding authors: blv@utdallas.edu (B. Lv); lyzhao@umich.edu (L. Zhao)

+ These authors contribute equally.

Abstract

Two-dimensional (2D) magnetism realized in van der Waals (vdW) materials has expanded to include a great variety of magnetic phases, over a short decade since its first discovery in 2016-2017. However, most of the investigated vdW magnets so far have highly symmetric crystal fields and isotropic in-plane lattice structures, making their 2D magnetism robust but often classical and expected. In this Perspective, we highlight a family of vdW magnets that have distorted crystal fields with low symmetries and orthorhombic crystal lattices with strong anisotropy, and furthermore, show their prospects for realizing a much richer landscape of magnetic phases and phase transitions. First, we introduce the classification of 2D vdW magnets based on their crystal fields and make a contrast between the orthorhombic vdW magnets of focus here and other popular honeycomb/hexagonal/kagome vdW magnets. We then discuss the material candidates, the emergent properties, and the designed controls for these orthorhombic 2D vdW magnets, using the representative CrSBr as an example and extending beyond it. Finally, we discuss a few existing challenges in orthorhombic 2D vdW magnets, overcome which would pave the way towards magneto-optical, opto-magnetic, and spintronic devices based on orthorhombic 2D vdW magnetism.

Main Text

For a two-dimensional (2D) system, orthorhombicity describes the differentiation between the two orthogonal in-plane directions. From a symmetry perspective, orthorhombic crystal system is one of the seven crystal systems [1], containing three structural point groups and nine magnetic point groups [2]. A key manifestation of structural orthorhombicity in 2D and quasi-2D materials is to introduce anisotropy in other physical properties spanning from electronic, magnetic, optical, *etc.*, to magneto-electric, opto-magnetic, opto-electronic, *etc.*, properties. One can see such a manifestation from two levels, *i.e.*, the interaction and the response. On the microscopic interaction level, it refers to the different electronic hopping, magnetic exchange, or light-matter interactions, *etc.*, between the two in-plane crystalline directions [3–6]. In the extreme case, it is possible to have strong interaction along one direction and fully quenched interaction in the orthogonal direction, making a structurally 2D system effectively one-dimensional (1D) in certain physical properties [7–11]. On the macroscopic response level, it leads to the contrasting behaviors between the two in-plane crystalline axes even under equivalent external stimuli along these two axes. As a result, it often leads to highly directional responses that are desired in various device applications [6,12–14].

2D antiferromagnetism (AFM) and ferromagnetism (FM) in van der Waals (vdW) materials were first discovered in monolayer FePS₃ in 2016 [15,16] and monolayer CrI₃ [17] and few-layer CrGeTe₃ [18] in 2017, which marks the opening of the blooming field of 2D magnetism [19–21]. They have served as a platform to investigate phase transitions in the 2D limit and explore potential new phases of matter [22], offered the magnetic ingredient to construct novel heterostructures and exploit its proximity effect [23,24], and further provided ample opportunities to implement the concept of 2D magnet-based micro-spintronic devices [25]. All of these have motivated the rapid expansion of the 2D vdW magnet pool, and as of now, it includes 3*d* and 4*d* transition metal halides [26–36], 3*d* transition metal chalcogenides [37–

44], ternary 3d transition metal compounds [15,16,18,45–62], Fe_nGeTe_2 ($3 \leq n \leq 5$) [63,64], $\text{MnBi}_{2n}\text{Te}_{3n+1}$ ($n = 1,2,3,4$) [65–70], and even 5d- and f-electron based compounds [71–75].

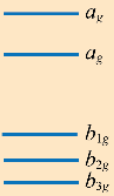
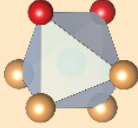
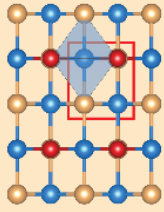
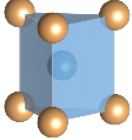
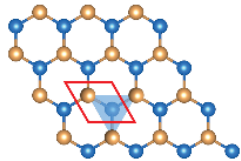
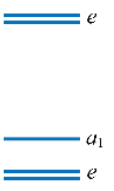
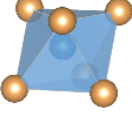
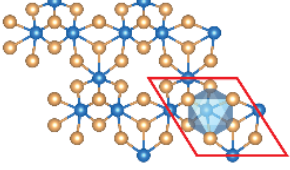
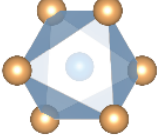
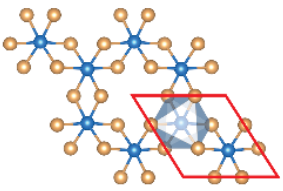
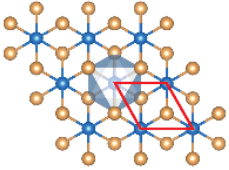
crystal field symmetry	energy levels	materials	building block	atomic lattice
C_{2v}		$\text{MXY} \begin{cases} \text{M} = \text{Ti, V, Cr, Fe} \\ \text{X} = \text{O, S, Se, Te} \\ \text{Y} = \text{Cl, Br, I} \end{cases}$		Orthorhombic 
D_{3h}		$2\text{H-phase MX}_2 \begin{cases} \text{M} = \text{V, Cr, Mn, Co} \\ \text{X} = \text{S, Se, Te} \end{cases}$		Honeycomb 
C_{3v}		$\text{Nb}_3\text{X}_8 \text{ (X = Cl, Br, I)}$		Kagome 
O_h		$\text{MX}_3 \begin{cases} \text{M} = \text{V, Cr, Mn}^*, \text{Fe}^*, \text{Ni}^* \\ \text{X} = \text{Cl, Br, I} \end{cases}$ $\text{MX}_2 \begin{cases} \text{M} = \text{V, Cr, Mn, Fe, Co, Ni} \\ \text{X} = \text{Cl, Br, I} \end{cases}$ $1\text{T-phase MX}_2 \begin{cases} \text{M} = \text{V, Cr, Mn, Co} \\ \text{X} = \text{S, Se, Te} \end{cases}$ $\text{CrXTe}_3 \text{ (X = Si, Ge, Sn)}$ $\text{MPX}_3 \begin{cases} \text{M} = \text{V, Cr, Mn, Fe, Co} \\ \text{X} = \text{S, Se, Te} \end{cases}$ $\alpha\text{-RuX}_3 \text{ (X = Cl, Br, I)}$ Fe-Ge-Te compounds Mn-Bi-Te compounds		Honeycomb  Hexagonal 

Figure 1 | Classification of 2D magnets based on their crystal fields and crystalline lattices. From the left to the right, each column represents the crystal field symmetry, the d -orbital degeneracy lifting under the crystal field, the discovered 2D magnetic materials, the atomic building block, and the lattice structure with the corresponding crystal system labeled. The red rectangle and parallelograms mark the unit cells.

A quick examination of the 2D vdW magnet pool reveals that most of their monolayer crystal lattices belong to the trigonal and the hexagonal crystal systems with in-plane isotropy (see **Figure 1**). In contrast to this majority, one family of 2D vdW magnets, MXY, stands out due to their orthorhombic

crystalline lattices that allow for in-plane anisotropy, where M = transition metals, X = chalcogens, and Y = halogens. The well-known member of this family is CrSBr [76,77], which hosts a quasi-1D conduction band [77–79], a robust layered AFM order [61,80], a rich magnetic phase diagram [61,81–85], exceptionally strong light-matter coupling [86–91], giant exciton binding energy [80,92–96], and linearly polarized photoluminescence [79,89,92], as well as air stability and high Néel temperature [61,78,80–82,84,85,97–100]. A peek into these distinctive properties of CrSBr, most of which originate from the structural orthorhombicity, which convinces us and invites us to explore MXY, the family of orthorhombic vdW magnets.

Classification of 2D vdW magnets based on crystal fields

The crystal lattice of a 2D vdW magnet is closely tied with its building block, which is the magnetic transition metal cation situating inside a cage made of ligand anions. Locally at the transition metal site, the d orbitals will experience the electrostatic potential created by the ligand cage, and as a result, its 5-fold degeneracy will be lifted in different ways depending on the symmetry of the cage. This crystal field effect is crucial in determining the spin state of the transition metal cation, the single ion and the exchange magnetic anisotropies for the 2D vdW magnet [101–103]. The crystal field is classified upon the point symmetry group at the transition metal site, and the common ones include the octahedral O_h , distorted octahedral D_{2h} or C_{2v} , trigonal prismatic D_{3h} , triangular prismatic C_{3v} , tetragonal T_d crystal fields, etc.

Nearly all vdW magnets thus far concern transition metals with d orbitals. **Figure 1** summarizes the crystal fields and the corresponding d orbital degeneracy lifting, with the vdW magnet candidates listed based on their crystal fields and crystal systems. From this summary, it is evident that most of the known vdW magnets have the O_h crystal field, the one with the highest symmetry and d orbitals splitting into the doubly degenerate e_g and triply degenerate t_{2g} manifolds. Following O_h , they are the D_{3h} and C_{3v} crystal fields with the e doublets protected by the 3-fold rotational symmetry. Finally, it is the D_{2h} and C_{2v} crystal field with the lowest symmetry and the fully lifted degeneracy for the d orbitals. It is also illuminating to notice that the vdW magnets with the 3-fold rotational symmetric crystal fields (*i.e.*, O_h , D_{3h} , C_{3v}) also fall into the isotropic crystal systems (*i.e.*, trigonal, hexagonal). Of interest to this Perspective is the family of MXY, which has the least symmetric C_{2v} crystal field and the anisotropic orthorhombic crystal system.

Distorted crystal field and orthorhombic lattice for enriched physical properties

The crystal structure of MXY is the same as that of CrSBr, each layer of which consists of transition metal monochalcogen MX double layer sandwiched between layers of halogen Y. The structural primitive cell contains two edge-sharing distorted octahedra, with one M^{3+} cation in the center and four X^{2-} and two Y^- anions at the vortices for each octahedron, which then arranges into an in-plane (ab -plane) orthorhombic network and further stacks vertically along the out-of-plane (c -axis) direction (**Figure 2**, center bottom) [80,104].

Within the distorted MXY octahedron, the coordination of two types of anions around the metal cation breaks the spatial inversion symmetry and leads to the low-symmetry C_{2v} crystal field. Comparing to the high-symmetry crystal fields, *e.g.*, O_h , D_{3h} , C_{3v} , this C_{2v} one has its own unique advantages. First, the C_{2v} crystal field fully lifts the orbital degeneracy of the five $3d$ orbitals, and thus is beneficial for stabilizing the spin state when tuning across $3d^1$ to $3d^5$ via changing M^{3+} from Ti^{3+} to Fe^{3+} [105–114]. This enables the possibility of exploring the magnetic phase diagram of varying spin states under the isostructural condition. Second, the strong distortion of the X_4Y_2 octahedral cage surrounding M^{3+} makes the electronic hopping and magnetic exchange coupling especially sensitive to the bond angles and length, and therefore empirically correlates the lattice, charge, and spin degrees of freedom (**Figure 2**, center middle).

This brings the opportunities of efficiently controlling the electronic and magnetic phases via applying static strain to the crystal lattice [115–123].

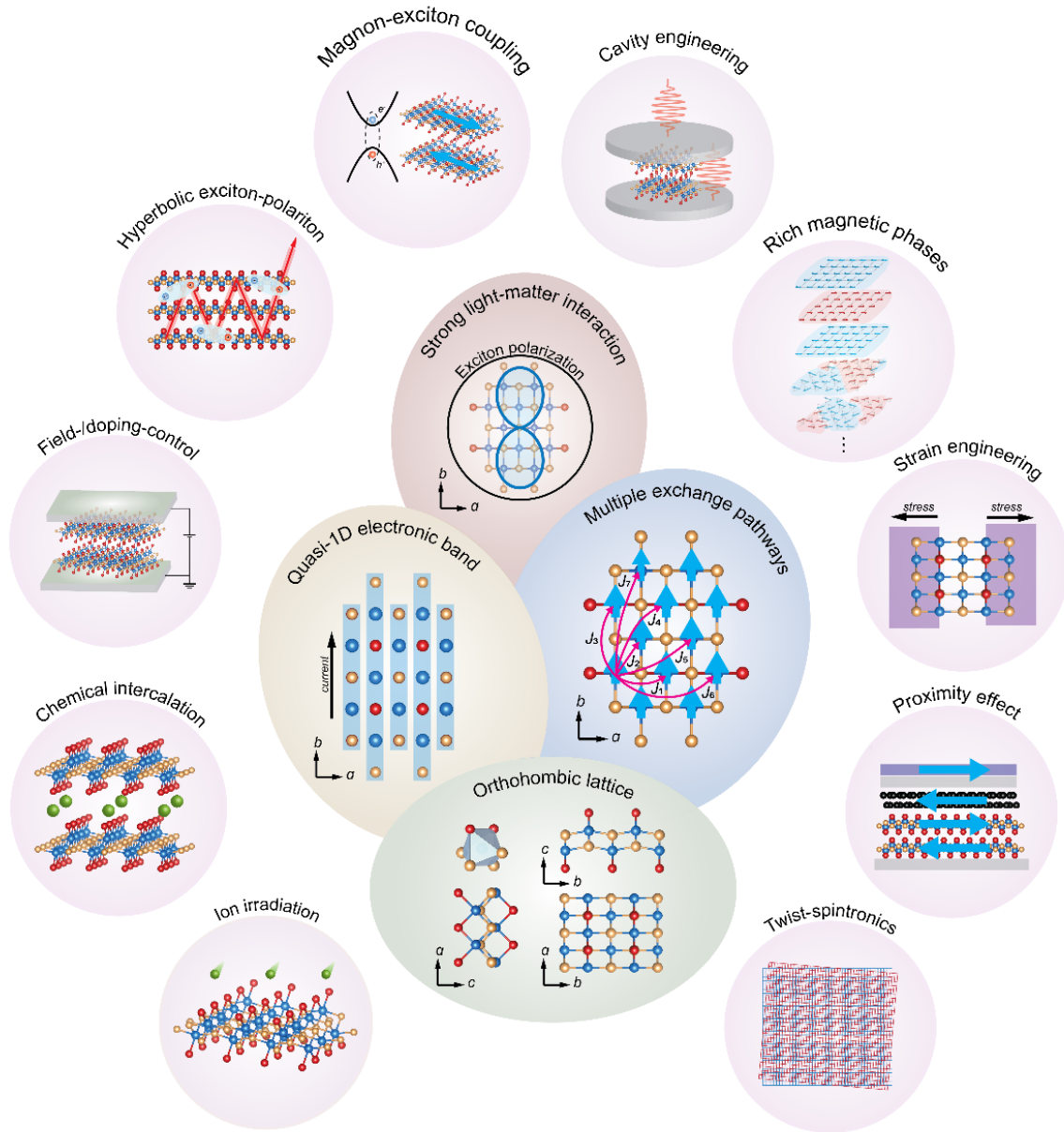


Figure 2 | Overview of key properties of 2D orthorhombic magnets and their associated opportunities. In the center, four unique physical properties of 2D orthorhombic magnets are shown, regarding the lattice, charge, and spin degrees of freedom and the coupling to light. In the outer shell, a series of research directions based on the four properties are highlighted.

The in-plane orthorhombic lattice of MXY can be seen from a different perspective – that is chains of metal cation M^{3+} with X^{2-}/Y^- ligands running along the a -axis to form ribbons of MXY and then these MXY ribbons connecting perpendicular to the a -axis to form a layer in the ab -plane. The M-M distance is $\sim 3\text{\AA}$ along the chain direction and $\sim 5\text{\AA}$ between ribbons, showing a clear, strong in-plane anisotropy for this orthorhombic crystal lattice. As compared to the in-plane isotropic crystal lattices, e.g., trigonal and hexagonal, this orthorhombic one brings distinct flavors. First, this in-plane lattice anisotropy can lead to

highly anisotropic electronic band dispersion (**Figure 2**, center middle), or even quasi-1D electronic band such as the case of CrSBr whose conduction band is only dispersive along $\Gamma - Y$ but dispersionless along $\Gamma - X$ [92–96,117,118,124]. Such a flatband further leads to exceptionally strong light-matter interactions in CrSBr in free space [86,92] and inside photonic cavities [87–91] (**Figure 2**, center top), which suggests that light and/or photonic cavities can be efficient knobs to tune the physical properties of MXY. Second, the structural and electronic anisotropies can further lead to different types and strengths of direct exchange and superexchange interactions along different crystal axes (**Figure 2**, center middle), and in the extreme limit, could lead to the quasi-1D spin chain state [107,125]. This offers an unprecedented opportunity of studying a full spectrum of dimensionality crossover from 3D to quasi-2D to 2D to quasi-1D. A survey of exciting research opportunities stemming from orthorhombic lattice, quasi-1D electronic band, complex magnetic exchange, and strong coupling to light are highlighted in the outer ring of **Figure 2**.

Material candidates of MXY vdW magnets

In principle, the family of MXY vdW magnets include $M = \text{Ti, V, Cr, Mn, and Fe}$; $X = \text{O, S, Se, and Te}$; and $Y = \text{Cl, Br, and I}$. In practice, the oxyhalides, $X = \text{O}$, contribute the largest group of compounds that have been successfully synthesized, whereas the $X = \text{S}$ group has CrSBr, and the $X = \text{Se, Te}$ groups have no known compounds in the single crystal form thus far (**Figure 3**).

For the $X = \text{O}$ group, the magnetic transition metal cation M^{3+} varies from Ti^{3+} to V^{3+} , Cr^{3+} , and Fe^{3+} , and hence allows for the $3d$ electron configurations from d^1 to d^2 , d^3 , and d^5 . We note that there has been no report on MnOY with the Mn^{3+} cation and the d^4 configuration, possibly due to the disproportionation reaction from Mn^{3+} to more stable Mn^{2+} and Mn^{4+} cations. The research on transition metal oxyhalides started with the synthesis of magnetic transition metal oxychlorides (MOCl with $M = \text{Ti, V, Cr, and Fe}$) by Schafer *et al* back in the late 1950s to the early 1960s [126–129], and then was further pursued in detailed structural analysis in the late 1970s [130–132], nearly two decades after the initial synthesis. It was until the recent 2000s when comprehensive magnetic and transport measurements were carried out for these oxychlorides polycrystals and single crystals [105,108–110,114,133–135], and even more recently in the 2020s when their magnetic properties in the 2D limit are explored [136,137]. In sharp contrast to oxychlorides (MOCl), oxybromides (MOBr) and oxyiodides (MOI) were much less studied, with only a couple of structural and magnetic characterizations for TiOBr in the early 2000s [125,138]. It is an interesting topic to investigate the magnetism evolution upon the variation of transition metal cations and the halogen anions in MOY.

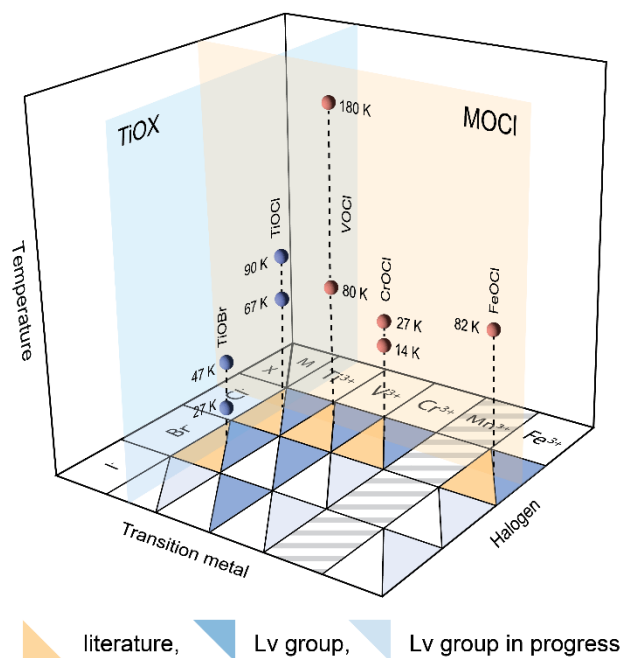


Figure 3 | Summary of magnetic phase transitions in MOY. A table of possible MOY magnetic materials is shown, with the literature reported ones marked in orange, the Lv group synthesized ones marked in blue, and the Lv group in progress ones marked in lighter blue. Magnetic phase transitions as a function of temperature are shown for the families of MOCl ($M = \text{Ti, V, Cr, Fe}$) and TiOY ($Y = \text{Cl, Br}$).

Let's first take oxychlorides as an example to see the effect of transition metal cations (**Figure 3**). TiOCl first undergoes a magnetic phase transition across $T_{c1} = 90$ K into an incommensurate spin state and then a first-order phase transition at $T_{c2} = 67$ K into a spin-Peierls state, both of which manifests as anomalies in temperature dependent magnetic susceptibility [105–107]. VOCl was reported to have a first magnetic phase transition at $T_{c1} = 180$ K whose nature remains elusive and unexplored [109] and then a second magnetic transition at $T_{c2} = 80$ K into an AFM state with a concurrent monoclinic structural distortion [108,109]. CrOCl also experiences two magnetic phase transitions, a higher one at $T_{c1} = 27$ K that is possibly due to an incommensurate magnetic order and a lower one at $T_{c2} = 14$ K that is for an AFM order accompanied with a monoclinic structural transition [110]. FeOCl transitions into an AFM state at $T_c = 82$ K together with a monoclinic structural distortion [98]. The spin-Peierls state in TiOCl and the monoclinic structural transition together with the AFM order in VOCl, CrOCl and FeOCl suggest the strong magnetoelastic coupling present in this group of oxychlorides [110,114,135], echoing that strain shall be a promising control knob for the magnetism in MOCl. Furthermore, the two magnetic phase transitions in TiOCl, VOCl, and CrOCl, together with the metamagnetic phase transitions found in CrOCl under the magnetic field [113], indicate the strong magnetic frustrations in MOCl, providing a new platform to investigate the interplay amongst geometric frustration, critical fluctuations, and collective phenomena in the 2D limit.

Let's then take a look at the effect of halogen ligand anions on the magnetism, where TiOY (Y = Cl, Br, I) is used as an example (**Figure 3**). TiOBr host a similar process of two magnetic phase transitions as TiOCl, but at lower critical temperatures of $T_{c1} = 47$ K into an incommensurate magnetic order and $T_{c2} = 27$ K into a spin-Peierls state [139]. TiOI has been hardly synthesized thus far. The similarity in magnetic phase transitions between TiOCl and TiOBr suggests the robustness of the magnetism to the halogen ligand anions.

For the X = S group, the only known compound is CrSBr [61,80,104], the material that has motivated this perspective. CrSBr undergoes a multi-stage magnetic phase transition process to enter the layered AFM order [61,82,100], supports the long-sought extraordinary phase transition [83], hosts a quasi-1D electronic conduction band [77–79,93–96], anisotropic excitons and polaritons [86–92,140], and strong spin-exciton coupling [89–91,140–144] (see details in the section of Emergent Properties in MXY vdW Magnets), as well as responding sensitively to external controls including strain [115,117–123], pressure [145,146], doping [147,148], electric field [149], twist [150–152], intercalation [153,154], ion and electron irradiation and implantation [124,155,156], etc. (see details in the section of Designed Controls over MXY vdW Magnets).

For the X = Se, Te groups, there has been no successful synthesis thus far. **Figure 3** summarizes the synthesis of MXY vdW magnets that have been reported in literature and/or produced by the Lv group.

Emergent properties in MXY vdW magnets

The distorted crystal field and the anisotropic orthorhombic lattice prepare MXY vdW magnets with a variety of exciting emergent properties. CrSBr is the most investigated member of the family thus far, and it has already shown distinct electronic, excitonic, polaronic, and magnetic properties.

Quasi-1D electronic conduction band. CrSBr is a semiconductor with the Fermi level lying within the semiconducting gap. Angle resolved photoemission spectroscopy (ARPES) can only access the electronic conduction band of CrSBr when CrSBr is doped by electrons, for example, through the charge transfer between the CrSBr flake and a metallic Ag(111) or Au(111) substrate [95] or the surface doping by the deposition of K atoms [93]. For the K-doped CrSBr bulk, the electronic conduction band is nearly dispersionless along the $\Gamma - X$ direction, but clearly dispersive along the $\Gamma - Y$ direction, as shown in **Figure 4a**, which is direct evidence of the quasi-1D nature and the flat-band character of the conduction band. It is further worth noting that the electron doping in CrSBr does more than simply raising the Fermi

level – it causes a significant reduction of the electronic band gap in the K-doped CrSBBr [93] and even drives a Lifshitz transition for the electronic band of CrSBBr flake on Ag (111) [95].

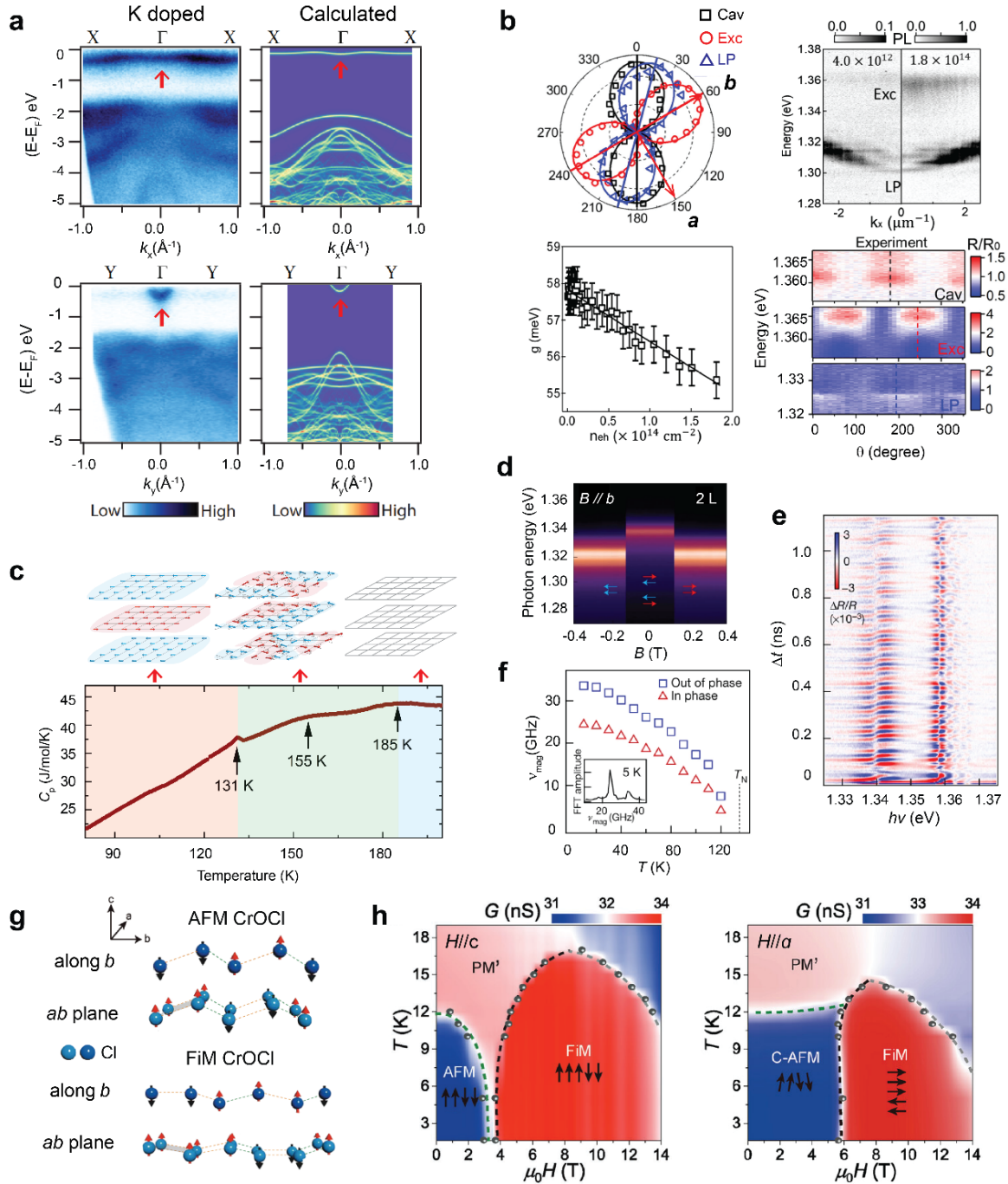


Figure 4 | Emergent properties in MXY vdW magnets. a. Quasi-1D electronic band of K-doped CrSBBr that is measured by ARPES and compared with theoretical calculations [93]. **b.** Linear polarization of the exciton emission in CrSBBr and strong light-matter coupling of CrSBBr integrated into photonic cavities [89]. **c.** Multi-stage magnetic phase transitions in bulk CrSBBr shown by the heat capacity measurements [82]. **d-f.** Strong charge-spin coupling shown in CrSBBr through the exciton energy shift upon the layer AFM to FM phase transition (d) [92] and the coherent population of magnons (e, f) [141]. **g-h.** Complex magnetism and magnetic phase diagram of CrOCl [113]. The figures in (a-h) are adapted from Refs. [93,89,82,92,141,113].

Anisotropic excitons and polaritons. The quasi-1D electronic conduction band readily contributes to the giant binding energy [80,92–96], the large oscillator strength [89], and the strong linear polarization of excitons in CrSBr [79,88,89,91,91,92,140]. Despite the variation in the electronic bandgap reported in literature using STM [79,80], ARPES [93–96], and optics [91,92], the photoluminescence frequency of CrSBr excitons is consistently within the range of 1.25–1.38 eV [79,80,91,92,140,141,144,147,157,158] and its polarization is highly linear along the b -axis direction [79,88,89,91,91,92,140] (**Figure 4b**). Integrating the CrSBr flakes into photonic cavities, exciton-polaritons emerge with a strong exciton-photon coupling strength that brings the system into the strong-coupling regime and with an exceptionally large Rabi splitting that is greater than any known systems to date [86–89] (**Figure 4b**). Furthermore, the polarization of the exciton-polariton inherits the linear polarization from the exciton, and at the same time, can be tuned by the photonic cavity polarization (**Figure 4b**) [89].

Multi-stage magnetic phase transitions. The magnetic ground state of bulk and few-layer CrSBr is the layered AFM order where the spins align ferromagnetically along the b -axis within the layer and antiferromagnetically between the adjacent layers (**Figure 4c**) [61,80,100,104]. The Néel temperature for bulk CrSBr is $T_{N,bulk} = 132$ K confirmed by the heat capacity and the magnetic susceptibility measurements [61,80,82,85,104]. Prior to $T_{N,bulk}$, three more characteristic temperature scales have been found for bulk CrSBr, $T_{N,surf} = 140$ K as the critical temperature for the surface layered AFM order [83], $T^* = 155$ K as a characteristic temperature for either a c -axis incoherent ferromagnetic order or a short-range layered AFM order [61,82,83,100], and $T^{**} = 180$ K as a temperature scale for the development of spin-spin correlations [82] (**Figure 4c**). Such a rich multi-stage magnetic phase transition process distinguishes CrSBr from many honeycomb and hexagonal vdW magnets. Surprisingly, when thinning down CrSBr to the 2D limit, the magnetic critical temperature increases, $T_{N,2L} = 140$ K for bilayer CrSBr and potentially $T_{C,1L} = 146$ K for monolayer CrSBr [61,85]. This counter-intuitive trend of the magnetic onset temperature with respect to the layer number remains to be explored. At $T_F = 30$ -40 K, there are reports of a ferromagnetic phase transition, whose origin is still under debate [81,85,98,159].

Strong charge-spin coupling. The spin and charge degrees of freedom are strongly coupled in CrSBr. The exciton energy has been shown to depend on the interlayer magnetic order, being 1.34 eV in the layered AFM phase and shifting down to 1.32 eV in the FM phase in bilayer CrSBr (**Figure 4d**) [92]. This sensitive dependence of exciton energy on the interlayer spin alignment further leads to an exciton frequency oscillation for about 4 meV when the spin waves are coherently excited (**Figure 4e**) [141]. Two spin wave modes were captured, one at 24 GHz for the in-phase spin precession between adjacent layers and the other at 34 GHz for the out-of-phase counterpart (**Figure 4f**) [141,160–162]. Given the large mismatch in energy between excitons and magnons, such a strong coupling between the two types of quasiparticles is exceptional.

Magnetic frustration and metamagnetism. In addition to CrSBr, CrOCl receives increasing attention lately. Different from CrSBr, CrOCl realizes an AFM order within the layers that has a slightly complicated AFM spin arrangement of $\uparrow\uparrow\downarrow$ along the b -axis and a FM chain along the a -axis (**Figure 4g**) [112,163]. Such an intralayer AFM order is a direct consequence of the geometrical frustration of spins, which is why this AFM transition is accompanied by a monoclinic structural distortion [110,113]. Furthermore, this geometric frustration leads to metamagnetic phases (**Figure 4h**) [111,113] and even a liquid-gas type phase transition when an external magnetic field is applied, suggesting a rich magnetic landscape for CrOCl, or more broadly, for the oxychloride group.

Designed controls over MXY vdW magnets

The intimate coupling between the lattice, charge, and spin degrees of freedom in MXY suggests diverse possibilities for controlling the physical properties of MXY. For example, from the lattice perspective, one

can use strain or pressure to modify the atomic structure or twist to introduce the superlattice; from the charge perspective, one can use electric field effect or chemical intercalation to tune the charge carrier density; from the spin perspective, one can use electric field to couple into the parity broken magnetic state or magnetic field to control the spins directly. In fact, these external controls have been successfully practiced in CrSBr.

Uniaxial strain. The complex magnetic exchange pathways and the magnetic anisotropies of CrSBr are highly sensitive to the in-plane lattice constants. A uniaxial strain device provides an efficient way to modify the lattice constants and therefore the magnetic properties. By applying a uniaxial strain along the *a*-axis of a ~20 nm CrSBr flake, a magnetic phase transition from the layered AFM to FM happens at a critical strain of 1.5% (**Figure 5a**), showing the strain-induced modification of interlayer exchange coupling. Moreover, this tensile strain also causes a significant reduction in the anisotropy energy and tunes the higher order magnetic anisotropies [115], for which one anticipates the modification in spin waves although not yet shown. This strain-driven layered AFM to FM transition further enables the strain-programmable magnetic tunneling junction, where the CrSBr serves as the tunneling barrier and its high and low tunneling resistance states are switched via the tensile strain [164].

Hydrostatic pressure. While the uniaxial strain makes a significant impact on the interlayer exchange coupling, hydrostatic pressure aims to affect the intralayer exchange coupling. A compression of the lattice under hydrostatic pressure is shown to reduce the magnetic critical temperature at a rate of -12.6 K/GPa because of the suppression of intralayer FM coupling, while the intralayer FM and interlayer AFM orders are maintained within the achievable pressure range (**Figure 5b**) [146]. The overall impact of hydrostatic pressure is less prominent as compared to the uniaxial strain, for the case of CrSBr.

Twisted superlattice. The twist between two atomic layers produces a superlattice out of the interference between the two angular mismatched atomic lattices. It has been introduced to tune the charge degree of freedom in twisted graphene and twist transition metal dichalcogenide structures [165–168] and more recently, applied to modify the spin degree of freedom in twisted 2D magnets [169–172], all of which have been limited to honeycomb lattice. Twisted CrSBr bilayers differ from them, because of their orthorhombic atomic lattice. It has already been shown in 90° twisted CrSBr bilayers that metamagnetic phases develop, showing hysteric behaviors and multistep magnetization switching under the magnetic field – which are features absent in natural bilayer CrSBr (**Figure 5c**) [150]. Moreover, it has been recently demonstrated that twisted CrSBr features a unique all-AFM tunneling junction with a high tunneling magnetoresistance ratio [151].

Electric field effect doping. The 2D nature of CrSBr flakes naturally allows for carrier doping through the electric field effect. Indeed, such an electrostatic control has been practiced in few-layer CrSBr to modulate their excitonic and magnetic properties (**Figure 5d**) [147]. Because of charge carrier doping, charged exciton complex forms in bilayer and trilayer CrSBr, and it exhibits strong coupling with the magnetic order just like the neutral exciton does. Furthermore, in the field-effect device geometry, metamagnetic phases have been predicted and observed in few-layer CrSBr [147–149].

Chemical intercalations. Chemical intercalation with alkali elements can achieve a higher level of electron doping than the popular field effect electric gating can do. In the case of CrSBr, Lithium intercalation has been shown to greatly enhance the magnetic onset temperature while maintaining the triaxial magnetic anisotropy (**Figure 5e**). In addition, a quasi-1D charge density wave emerges upon Lithium intercalation and persists above the magnetic transition temperature [153]. A more recent work by the Lv and Zhao group further shows that tetrabutylammonium (TBA⁺) interaction into CrSBr can significantly modulate the magnetic and transport properties (**Figure 5f**) [173].

Electric field. The magnetoelectric effect of the layered AFM state in CrSBr allows for the electric field control over the magnetism. Taking bilayer CrSBr, the layered AFM order breaks both spatial-inversion (P) and time-reversal (T) symmetries but preserves their product (PT) symmetry, allowing for the

direct coupling between the P-odd electric field and this PT-symmetric AFM order. While this has not been demonstrated in bilayer CrSBr, it has been shown in bilayer CrI₃ that also hosts the PT-symmetric layered AFM order [174,175].

Magnetic field. The magnetic field can be used to compete with the interlayer AFM coupling and the triaxial anisotropy in CrSBr, as well as modifying the geometric frustration and suppressing the spin fluctuations in CrOCl. In the case of natural CrSBr, it drives the layered AFM to FM spin flip transition with the magnetic field along the *b*-axis to overcome the interlayer AFM coupling and causes the spin canting transitions into the FM state with the field along the *a*- and *c*-axes to counteract the magnetic anisotropies (**Figure 5g**) [80,176,177]. Under the applied magnetic field, metamagnetic phase transitions can also be induced in CrOCl (**Figure 5h**).

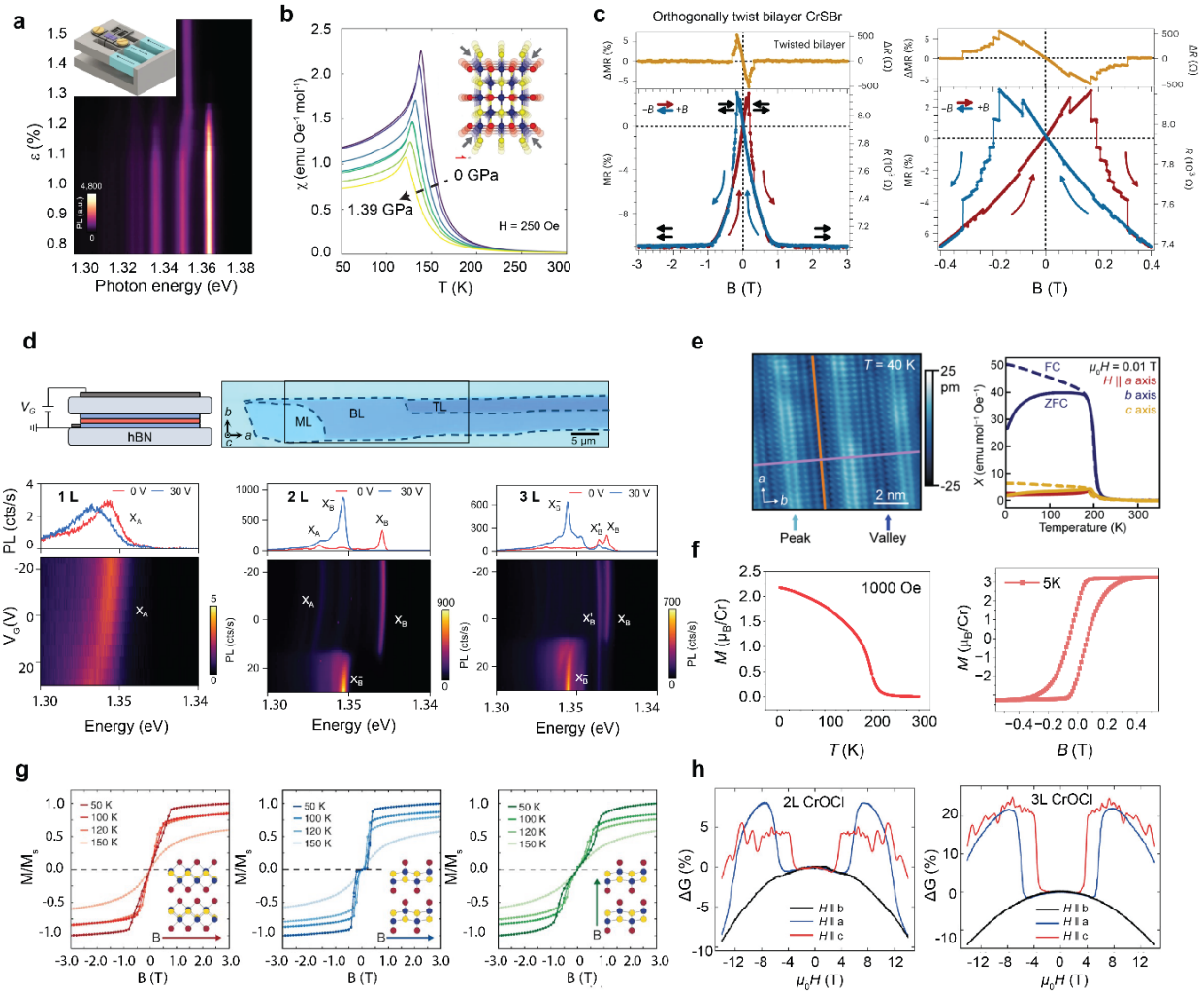


Figure 5 | Designed controls over MXY vdW magnets. **a.** Static strain control over the magnetism and excitons in CrSBr thin layers [115]. **b.** Hydrostatic pressure control of the magnetic properties in bulk CrSBr [146]. **c.** Twisting engineering the magnetic properties in twisted CrSBr homostructures [150]. **d.** Electrostatic doping effect in modifying the magnetism and excitons in CrSBr flakes [147]. **e.** Li intercalation for introducing charge density wave and increasing the magnetic onset temperature in Li-intercalated CrSBr bulk [153]. **f.** Organic molecule intercalation for altering the interlayer magnetic coupling from AFM to FM and enhancing the magnetic onset temperature [173]. **g.** Magnetic field-induced magnetic phase transitions in CrSBr bulk [80]. **h.** Metamagnetic phase transitions induced by applied magnetic fields in 2L and 3L CrOCl [113]. The figures in (a-h) are adapted from Refs. [115,146,150,147,153,173,80,113].

Challenges and outlook of MXY 2D vdW magnetism

The unique lattice characters of MXY vdW magnets, *i.e.*, distorted low-symmetry crystal field and orthorhombic anisotropy atomic lattice, bestow intriguing electronic, magnetic, and optical properties that can be exploited for future spintronic, magneto-optical, or opto-magnetic devices. Yet, these prospects of MXY vdW magnets heavily rely on the crystalline quality, the comprehensive understanding, and the integration flexibility of MXY. In this section, we comment on existing challenges in these three aspects.

Crystalline quality. In general, the crystalline quality of 2D magnets is poorer than that of graphene and transition metal dichalcogenide. For MXY, there are several types of defects of concern. First, the halogen deficiency often happens, for example, the Br vacancies in CrSBr [156,159]. These defects may act as trapping sites for charge carriers, and therefore, make the electric doping inefficient. They also interrupt the magnetic exchange pathways and impact the magnetic properties. Such halogen defects could be even more severe in the oxybromide and oxyiodide due to the large size and electronegativity difference between oxygen and Br/I. Second, the halogen and chalcogen inter-site mixing could happen, especially for those oxyhalide pairs with rather close anion size and electronegativity such as Se-Br, S-Cl and Te-I. In fact, site mixing has been observed in Cr₃Se₂Br₅ [178] and Bi₄Cl₂S₅ [179], which might be the root cause preventing the successful single crystal synthesis of CrSeBr and CrSCl. Finally, the mixed phases of different chemical ratios can happen, for example, for the case of VOCl with the possibility of VOCl₂, VO₂Cl and VOCl₃ [180]. It is worth noting that defects play a more profound role in magnetism, or more generally, ordering phenomena, in 2D than 3D. Therefore, novel crystal growth strategies and dedicated materials handling processes have to be developed to ensure the access of intrinsic properties of 2D MXY magnetism and to allow for efficient electrostatic device controls.

Comprehensive probes. Currently, 2D magnetism is primarily probed by optical spectroscopy and spin transport measurements, mainly because the small sample volume excludes many bulk probes. For example, in 2D CrSBr, the magnetic states are mostly inferred from the exciton spectra relying on the coupling between the exciton and magnetic order [91,92,140,144,147], and sometimes analyzed through the second harmonic generation thanks to its sensitivity to point symmetries [61,82,83,177]. However, a comprehensive understanding of magnetism requires the identification of its accurate space group (including both point and translational symmetries), its complete spin wave dispersion, its real space imaging of spin textures, magnetic domains, and domain walls, *etc.* which optics and spin transport cannot provide. It calls for techniques of spin sensitivity and with momentum and/or spatial resolutions to complement optics and transport in the research of 2D magnetism including and beyond MXY. For the momentum resolution, resonant x-ray spectroscopy is gradually applied in studying 2D magnets [181]. For the spatial resolution, scanning NV microscopy [182,183], spin-resolved scanning tunneling microscopy [184], Lorentz transmission electron microscopy [185] and phase-resolved second harmonic generation [177] are introduced in imaging 2D magnets lately.

Integration flexibility. It is highly desirable to harvest the intriguing physical properties of MXY by embedding them into devices. MXY is especially appealing in this regard, because first their properties can support a diverse variety of devices, including spintronics, magneto-optics, opto-magnetics, and even optoelectronics [151,186,187]. Second their vdW 2D nature allows for ultraclean interfaces and ultracompact arrangement of the device structures. And third their air stability is superb compared to many other 2D magnets. However, it is nearly impossible to scale up if relying on mechanical exfoliation to provide the 2D MXY vdW flakes. Yet, there have been no successful efforts on large-scale thin film growth even for CrSBr, the most investigated MXY family member. This possibly roots in the complication involved in handling the potentially toxic and corrosive precursors and gases during the film deposition. On the other hand, large area highly crystalline thin film growth of oxyhalides appears to be feasible with solid state metal oxides and metal halides under reduced oxygen atmosphere, as it has been demonstrated in the similar phase BiOI and LaOCl thin film growth recently [188–190].

Acknowledgements

L. Z. and X. G. acknowledge the support from the Department of Energy Office of Basic Science under Award DE-SC0024145 (for the discussions on twisted and moiré magnetism), the National Science Foundation under Award DMR-174774, DMR-2103731, and MRSEC DMR-2309029, the Air Force Office of Scientific Research under Award FA9550-21-1-0065, the Office of Naval Research under Award N00014-21-1-2770, the Gordon and Betty Moore Foundation under Grant N031710, and the Alfred P. Sloan Foundation (for the discussions on natural 2D magnetism). B. L. and W. L. acknowledges the support from US Air Force Office of Scientific Research Grant No. FA9550-19-1-0037, National Science Foundation-DMREF-2324033 and Office of Naval Research grant no. N00014-23-1-2020 and N00014-22-1-2755.

Author Information

These authors contribute equally: Xiaoyu Guo, Wenhao Liu.

Authors and Affiliations

Department of Physics, the University of Michigan, Ann Arbor, MI, 48109, USA

Xiaoyu Guo, Liuyan Zhao

Department of Physics, the University of Texas at Dallas, Richardson, TX 75080, USA

Wenhao Liu, Bing Lv

Corresponding Authors

Correspondence to Liuyan Zhao (lyzhao@umich.edu), or Bing Lv (blv@utdallas.edu)

Competing Interests

The authors declare no competing interests.

References

- [1] N. W. Ashcroft and N. D. Mermin, *Solid State Physics* (Saunders college publishing, United States, 1976).
- [2] R. R. Birss, *Symmetry and Magnetism* (North-Holland Pub. Co., Amsterdam, 1966).
- [3] X. Ling, H. Wang, S. Huang, F. Xia, and M. S. Dresselhaus, The renaissance of black phosphorus, *Proc. Natl. Acad. Sci.* **112**, 4523 (2015).
- [4] A. Carvalho, M. Wang, X. Zhu, A. S. Rodin, H. Su, and A. H. Castro Neto, Phosphorene: from theory to applications, *Nat. Rev. Mater.* **1**, 16061 (2016).
- [5] A. S. Sarkar and E. Stratakis, Recent Advances in 2D Metal Monochalcogenides, *Adv. Sci.* **7**, 2001655 (2020).
- [6] J. O. Island et al., Electronics and optoelectronics of quasi-1D layered transition metal trichalcogenides, *2D Mater.* **4**, 022003 (2017).
- [7] F. Levkovich-Maslyuk, The Bethe ansatz, *J. Phys. Math. Theor.* **49**, 323004 (2016).
- [8] I. A. Zaliznyak, A glimpse of a Luttinger liquid, *Nat. Mater.* **4**, 273 (2005).
- [9] X. Du et al., Crossed Luttinger liquid hidden in a quasi-two-dimensional material, *Nat. Phys.* **19**, 40 (2023).
- [10] J. Yu et al., Giant nonlinear optical activity in two-dimensional palladium diselenide, *Nat. Commun.* **12**, 1083 (2021).

- [11] J. Gooth et al., Axionic charge-density wave in the Weyl semimetal $(\text{TaSe}_4)_2\text{I}$, *Nature* **575**, 315 (2019).
- [12] C. Gong and X. Zhang, Two-dimensional magnetic crystals and emergent heterostructure devices, *Science* **363**, eaav4450 (2019).
- [13] Y. Abate, D. Akinwande, S. Gamage, H. Wang, M. Snure, N. Poudel, and S. B. Cronin, Recent Progress on Stability and Passivation of Black Phosphorus, *Adv. Mater.* **30**, 1704749 (2018).
- [14] A. Patra and C. S. Rout, Anisotropic quasi-one-dimensional layered transition-metal trichalcogenides: synthesis, properties and applications, *RSC Adv.* **10**, 36413 (2020).
- [15] J.-U. Lee, S. Lee, J. H. Ryoo, S. Kang, T. Y. Kim, P. Kim, C.-H. Park, J.-G. Park, and H. Cheong, Ising-Type Magnetic Ordering in Atomically Thin FePS_3 , *Nano Lett.* **16**, 7433 (2016).
- [16] X. Wang et al., Raman spectroscopy of atomically thin two-dimensional magnetic iron phosphorus trisulfide (FePS_3) crystals, *2D Mater.* **3**, 031009 (2016).
- [17] B. Huang et al., Layer-dependent ferromagnetism in a van der Waals crystal down to the monolayer limit, *Nature* **546**, 270 (2017).
- [18] C. Gong et al., Discovery of intrinsic ferromagnetism in two-dimensional van der Waals crystals, *Nature* **546**, 7657 (2017).
- [19] K. S. Burch, D. Mandrus, and J.-G. Park, Magnetism in two-dimensional van der Waals materials, *Nature* **563**, 47 (2018).
- [20] M. Gibertini, M. Koperski, A. F. Morpurgo, and K. S. Novoselov, Magnetic 2D materials and heterostructures, *Nat. Nanotechnol.* **14**, 408 (2019).
- [21] Q. H. Wang et al., The Magnetic Genome of Two-Dimensional van der Waals Materials, *ACS Nano* **16**, 6960 (2022).
- [22] Z. Sun et al., Dimensionality crossover to a two-dimensional vestigial nematic state from a three-dimensional antiferromagnet in a honeycomb van der Waals magnet, *Nat. Phys.* **20**, 1764 (2024).
- [23] J.-F. Dayen, S. J. Ray, O. Karis, I. J. Vera-Marun, and M. V. Kamalakar, Two-dimensional van der Waals spinterfaces and magnetic-interfaces, *Appl. Phys. Rev.* **7**, 011303 (2020).
- [24] B. Huang, M. A. McGuire, A. F. May, D. Xiao, P. Jarillo-Herrero, and X. Xu, Emergent phenomena and proximity effects in two-dimensional magnets and heterostructures, *Nat. Mater.* **19**, 1276 (2020).
- [25] J. F. Sierra, J. Fabian, R. K. Kawakami, S. Roche, and S. O. Valenzuela, Van der Waals heterostructures for spintronics and opto-spintronics, *Nat. Nanotechnol.* **16**, 856 (2021).
- [26] A. Banerjee, J. Yan, J. Knolle, C. A. Bridges, M. B. Stone, M. D. Lumsden, D. G. Mandrus, D. A. Tennant, R. Moessner, and S. E. Nagler, Neutron scattering in the proximate quantum spin liquid $\alpha\text{-RuCl}_3$, *Science* **356**, 1055 (2017).
- [27] Y. Haraguchi, C. Michioka, M. Ishikawa, Y. Nakano, H. Yamochi, H. Ueda, and K. Yoshimura, Magnetic–Nonmagnetic Phase Transition with Interlayer Charge Disproportionation of Nb_3Cl_8 Trimers in the Cluster Compound Nb_3Cl_8 , *Inorg. Chem.* **56**, 3483 (2017).
- [28] M. A. McGuire, Crystal and Magnetic Structures in Layered, Transition Metal Dihalides and Trihalides, *Crystals* **7**, 5 (2017).
- [29] H. H. Kim et al., Evolution of interlayer and intralayer magnetism in three atomically thin chromium trihalides, *Proc. Natl. Acad. Sci.* **116**, 11131 (2019).
- [30] C. M. Pasco, I. El Baggari, E. Bianco, L. F. Kourkoutis, and T. M. McQueen, Tunable Magnetic Transition to a Singlet Ground State in a 2D van der Waals Layered Trimerized Kagomé Magnet, *ACS Nano* **13**, 9457 (2019).
- [31] H. Takagi, T. Takayama, G. Jackeli, G. Khaliullin, and S. E. Nagler, Concept and realization of Kitaev quantum spin liquids, *Nat. Rev. Phys.* **1**, 264 (2019).
- [32] S. Tomar, B. Ghosh, S. Mardanya, P. Rastogi, B. S. Bhadoria, Y. S. Chauhan, A. Agarwal, and S. Bhowmick, Intrinsic magnetism in monolayer transition metal trihalides: A comparative study, *J. Magn. Magn. Mater.* **489**, 165384 (2019).

- [33] F. Conte, D. Ninno, and G. Cantele, Layer-dependent electronic and magnetic properties of Nb_3I_8 , *Phys. Rev. Res.* **2**, 033001 (2020).
- [34] D. Soriano, M. I. Katsnelson, and J. Fernández-Rossier, Magnetic Two-Dimensional Chromium Trihalides: A Theoretical Perspective, *Nano Lett.* **20**, 6225 (2020).
- [35] Y. Imai et al., Zigzag magnetic order in the Kitaev spin-liquid candidate material RuBr_3 with a honeycomb lattice, *Phys. Rev. B* **105**, L041112 (2022).
- [36] D. Ni, X. Gui, K. M. Powderly, and R. J. Cava, Honeycomb-Structure RuI_3 , A New Quantum Material Related to $\alpha\text{-RuCl}_3$, *Adv. Mater.* **34**, 2106831 (2022).
- [37] C. Ataca, H. Şahin, and S. Ciraci, Stable, Single-Layer MX_2 Transition-Metal Oxides and Dichalcogenides in a Honeycomb-Like Structure, *J. Phys. Chem. C* **116**, 8983 (2012).
- [38] A. Otero Fumega, J. Phillips, and V. Pardo, Controlled Two-Dimensional Ferromagnetism in 1T-CrTe_2 : The Role of Charge Density Wave and Strain, *J. Phys. Chem. C* **124**, 21047 (2020).
- [39] Y. Wang, J. Ren, J. Li, Y. Wang, H. Peng, P. Yu, W. Duan, and S. Zhou, Evidence of charge density wave with anisotropic gap in a monolayer VTe_2 film, *Phys. Rev. B* **100**, 241404 (2019).
- [40] J. Feng et al., Electronic Structure and Enhanced Charge-Density Wave Order of Monolayer VSe_2 , *Nano Lett.* **18**, 4493 (2018).
- [41] X. Zhang et al., Room-temperature intrinsic ferromagnetism in epitaxial CrTe_2 ultrathin films, *Nat. Commun.* **12**, 2492 (2021).
- [42] D. J. O'Hara et al., Room Temperature Intrinsic Ferromagnetism in Epitaxial Manganese Selenide Films in the Monolayer Limit, *Nano Lett.* **18**, 3125 (2018).
- [43] Z. Tang, Y. Chen, Y. Zheng, and X. Luo, Strain engineering magnetocrystalline anisotropy in strongly correlated VTe_2 with room-temperature ferromagnetism, *Phys. Rev. B* **105**, 214403 (2022).
- [44] M. Bonilla, S. Kolekar, Y. Ma, H. C. Diaz, V. Kalappattil, R. Das, T. Eggers, H. R. Gutierrez, M.-H. Phan, and M. Batzill, Strong room-temperature ferromagnetism in VSe_2 monolayers on van der Waals substrates, *Nat. Nanotechnol.* **13**, 289 (2018).
- [45] P. A. Joy and S. Vasudevan, Magnetism in the layered transition-metal thiophosphates MPS_3 ($\text{M}=\text{Mn, Fe, and Ni}$), *Phys. Rev. B* **46**, 5425 (1992).
- [46] P. Jeevanandam and S. Vasudevan, Magnetism in MnPSe_3 : a layered $3d^5$ antiferromagnet with unusually large XY anisotropy, *J. Phys. Condens. Matter* **11**, 3563 (1999).
- [47] M.-W. Lin et al., Ultrathin nanosheets of CrSiTe_3 : a semiconducting two-dimensional ferromagnetic material, *J. Mater. Chem. C* **4**, 315 (2015).
- [48] H. L. Zhuang, Y. Xie, P. R. C. Kent, and P. Ganesh, Computational discovery of ferromagnetic semiconducting single-layer CrSnTe_3 , *Phys. Rev. B* **92**, 035407 (2015).
- [49] G. T. Lin et al., Tricritical behavior of the two-dimensional intrinsically ferromagnetic semiconductor CrGeTe_3 , *Phys. Rev. B* **95**, 245212 (2017).
- [50] Z. Jiang, P. Wang, J. Xing, X. Jiang, and J. Zhao, Screening and Design of Novel 2D Ferromagnetic Materials with High Curie Temperature above Room Temperature, *ACS Appl. Mater. Interfaces* **10**, 39032 (2018).
- [51] H. Liu, J.-T. Sun, M. Liu, and S. Meng, Screening Magnetic Two-Dimensional Atomic Crystals with Nontrivial Electronic Topology, *J. Phys. Chem. Lett.* **9**, 6709 (2018).
- [52] Y. Guo, Y. Zhang, S. Yuan, B. Wang, and J. Wang, Chromium sulfide halide monolayers: intrinsic ferromagnetic semiconductors with large spin polarization and high carrier mobility, *Nanoscale* **10**, 18036 (2018).
- [53] N. Miao, B. Xu, L. Zhu, J. Zhou, and Z. Sun, 2D Intrinsic Ferromagnets from van der Waals Antiferromagnets, *J. Am. Chem. Soc.* **140**, 2417 (2018).
- [54] K. Kim, S. Y. Lim, J.-U. Lee, S. Lee, T. Y. Kim, K. Park, G. S. Jeon, C.-H. Park, J.-G. Park, and H. Cheong, Suppression of magnetic ordering in XXZ-type antiferromagnetic monolayer NiPS_3 , *Nat. Commun.* **10**, 1 (2019).

- [55] C. Wang, X. Zhou, L. Zhou, N.-H. Tong, Z.-Y. Lu, and W. Ji, A family of high-temperature ferromagnetic monolayers with locked spin-dichroism-mobility anisotropy: MnNX and CrCX (X = Cl, Br, I; C = S, Se, Te), *Sci. Bull.* **64**, 293 (2019).
- [56] G. Long, H. Henck, M. Gibertini, D. Dumcenco, Z. Wang, T. Taniguchi, K. Watanabe, E. Giannini, and A. F. Morpurgo, Persistence of Magnetism in Atomically Thin MnPS₃ Crystals, *Nano Lett.* **20**, 2452 (2020).
- [57] R. Han, Z. Jiang, and Y. Yan, Prediction of Novel 2D Intrinsic Ferromagnetic Materials with High Curie Temperature and Large Perpendicular Magnetic Anisotropy, *J. Phys. Chem. C* **124**, 7956 (2020).
- [58] S. Wang, J. Wang, and M. Khazaei, Discovery of stable and intrinsic antiferromagnetic iron oxyhalide monolayers, *Phys. Chem. Chem. Phys.* **22**, 11731 (2020).
- [59] J. Pan, J. Yu, Y.-F. Zhang, S. Du, A. Janotti, C.-X. Liu, and Q. Yan, Quantum anomalous Hall effect in two-dimensional magnetic insulator heterojunctions, *Npj Comput. Mater.* **6**, 1 (2020).
- [60] Z. Ni, A. V. Haglund, H. Wang, B. Xu, C. Bernhard, D. G. Mandrus, X. Qian, E. J. Mele, C. L. Kane, and L. Wu, Imaging the Néel vector switching in the monolayer antiferromagnet MnPSe₃ with strain-controlled Ising order, *Nat. Nanotechnol.* **16**, 7 (2021).
- [61] K. Lee, A. H. Dismukes, E. J. Telford, R. A. Wisconsin, J. Wang, X. Xu, C. Nuckolls, C. R. Dean, X. Roy, and X. Zhu, Magnetic Order and Symmetry in the 2D Semiconductor CrSBr, *Nano Lett.* **21**, 3511 (2021).
- [62] H. W. S. Arachchige, W. R. Meier, M. Marshall, T. Matsuoka, R. Xue, M. A. McGuire, R. P. Hermann, H. Cao, and D. Mandrus, Charge Density Wave in Kagome Lattice Intermetallic ScV₆Sn₆, *Phys. Rev. Lett.* **129**, 216402 (2022).
- [63] J. Seo et al., Nearly room temperature ferromagnetism in a magnetic metal-rich van der Waals metal, *Sci. Adv.* **6**, eaay8912 (2020).
- [64] H. Zhang et al., Itinerant ferromagnetism in van der Waals Fe_{5-x}GeTe₂ crystals above room temperature, *Phys. Rev. B* **102**, 064417 (2020).
- [65] J. Li, Y. Li, S. Du, Z. Wang, B.-L. Gu, S.-C. Zhang, K. He, W. Duan, and Y. Xu, Intrinsic magnetic topological insulators in van der Waals layered MnBi₂Te₄-family materials, *Sci. Adv.* **5**, eaaw5685 (2019).
- [66] C. Hu et al., Realization of an intrinsic ferromagnetic topological state in MnBi₈Te₁₃, *Sci. Adv.* **6**, eaba4275 (2020).
- [67] C. Hu et al., A van der Waals antiferromagnetic topological insulator with weak interlayer magnetic coupling, *Nat. Commun.* **11**, 97 (2020).
- [68] Y. Deng, Y. Yu, M. Z. Shi, Z. Guo, Z. Xu, J. Wang, X. H. Chen, and Y. Zhang, Quantum anomalous Hall effect in intrinsic magnetic topological insulator MnBi₂Te₄, *Science* **367**, 895 (2020).
- [69] C. Liu, Y. Wang, H. Li, Y. Wu, Y. Li, J. Li, K. He, Y. Xu, J. Zhang, and Y. Wang, Robust axion insulator and Chern insulator phases in a two-dimensional antiferromagnetic topological insulator, *Nat. Mater.* **19**, 522 (2020).
- [70] A. Gao et al., Layer Hall effect in a 2D topological axion antiferromagnet, *Nature* **595**, 521 (2021).
- [71] M. Ormaza et al., High Temperature Ferromagnetism in a GdAg₂ Monolayer, *Nano Lett.* **16**, 4230 (2016).
- [72] X.-L. Sheng and B. K. Nikolić, Monolayer of the 5d transition metal trichloride OsCl₃: A playground for two-dimensional magnetism, room-temperature quantum anomalous Hall effect, and topological phase transitions, *Phys. Rev. B* **95**, 201402 (2017).
- [73] S. Lei et al., High mobility in a van der Waals layered antiferromagnetic metal, *Sci. Adv.* **6**, eaay6407 (2020).
- [74] B. Wang, X. Zhang, Y. Zhang, S. Yuan, Y. Guo, S. Dong, and J. Wang, Prediction of a two-dimensional high-T_c f-electron ferromagnetic semiconductor, *Mater. Horiz.* **7**, 1623 (2020).
- [75] S. Mahatara and B. Kiefer, Layer dependent magnetism and topology in monolayer and bilayers ReX₃ (X = Br, I), *J. Phys. Condens. Matter* **33**, 455801 (2021).

- [76] M. E. Ziebel, M. L. Feuer, J. Cox, X. Zhu, C. R. Dean, and X. Roy, CrSBr: An Air-Stable, Two-Dimensional Magnetic Semiconductor, *Nano Lett.* (2024).
- [77] J. Klein and F. M. Ross, Materials beyond monolayers: The magnetic quasi-1D semiconductor CrSBr, *J. Mater. Res.* **39**, 3045 (2024).
- [78] F. Wu, I. Gutiérrez-Lezama, S. A. López-Paz, M. Gibertini, K. Watanabe, T. Taniguchi, F. O. von Rohr, N. Ubrig, and A. F. Morpurgo, Quasi-1D Electronic Transport in a 2D Magnetic Semiconductor, *Adv. Mater.* **34**, 2109759 (2022).
- [79] J. Klein et al., The Bulk van der Waals Layered Magnet CrSBr is a Quasi-1D Material, *ACS Nano* **17**, 5316 (2023).
- [80] E. J. Telford et al., Layered Antiferromagnetism Induces Large Negative Magnetoresistance in the van der Waals Semiconductor CrSBr, *Adv. Mater.* **32**, 2003240 (2020).
- [81] S. A. López-Paz, Z. Guguchia, V. Y. Pomjakushin, C. Witteveen, A. Cervellino, H. Luetkens, N. Casati, A. F. Morpurgo, and F. O. von Rohr, Dynamic magnetic crossover at the origin of the hidden-order in van der Waals antiferromagnet CrSBr, *Nat. Commun.* **13**, 4745 (2022).
- [82] W. Liu et al., A Three-Stage Magnetic Phase Transition Revealed in Ultrahigh-Quality van der Waals Bulk Magnet CrSBr, *ACS Nano* **16**, 15917 (2022).
- [83] X. Guo et al., Extraordinary phase transition revealed in a van der Waals antiferromagnet, *Nat. Commun.* **15**, 6472 (2024).
- [84] C. Ye et al., Layer-Dependent Interlayer Antiferromagnetic Spin Reorientation in Air-Stable Semiconductor CrSBr, *ACS Nano* **16**, 11876 (2022).
- [85] E. J. Telford et al., Coupling between magnetic order and charge transport in a two-dimensional magnetic semiconductor, *Nat. Mater.* **21**, 754 (2022).
- [86] F. L. Ruta et al., Hyperbolic exciton polaritons in a van der Waals magnet, *Nat. Commun.* **14**, 8261 (2023).
- [87] F. Dirnberger et al., Magneto-optics in a van der Waals magnet tuned by self-hybridized polaritons, *Nature* **620**, 7974 (2023).
- [88] T. Wang, D. Zhang, S. Yang, Z. Lin, Q. Chen, J. Yang, Q. Gong, Z. Chen, Y. Ye, and W. Liu, Magnetically-dressed CrSBr exciton-polaritons in ultrastrong coupling regime, *Nat. Commun.* **14**, 1 (2023).
- [89] Q. Li et al., Two-Dimensional Magnetic Exciton Polariton with Strongly Coupled Atomic and Photonic Anisotropies, *Phys. Rev. Lett.* **133**, 266901 (2024).
- [90] C. Li, C. Shen, N. Jiang, K. K. Tang, X. Liu, J. Guo, Y. Liang, J. Song, X. Deng, and Q. Zhang, 2D CrSBr Enables Magnetically Controllable Exciton-Polaritons in an Open Cavity, *Adv. Funct. Mater.* **34**, 2411589 (2024).
- [91] L. Nessi, C. A. Occhialini, A. K. Demir, L. Powalla, and R. Comin, Magnetic Field Tunable Polaritons in the Ultrastrong Coupling Regime in CrSBr, *ACS Nano* **18**, 34235 (2024).
- [92] N. P. Wilson et al., Interlayer electronic coupling on demand in a 2D magnetic semiconductor, *Nat. Mater.* **20**, 1657 (2021).
- [93] S. Smolenski et al., Large exciton binding energy in a bulk van der Waals magnet from quasi-1D electronic localization, *Nat. Commun.* **16**, (2024).
- [94] M. D. Watson, S. Acharya, J. E. Nunn, L. Nagireddy, D. Pashov, M. Rösner, M. van Schilfgaarde, N. R. Wilson, and C. Cacho, Giant exchange splitting in the electronic structure of A-type 2D antiferromagnet CrSBr, *Npj 2D Mater. Appl.* **8**, 54 (2024).
- [95] M. Bianchi et al., Charge transfer induced Lifshitz transition and magnetic symmetry breaking in ultrathin CrSBr crystals, *Phys. Rev. B* **108**, 195410 (2023).
- [96] M. Bianchi et al., Paramagnetic electronic structure of CrSBr: Comparison between ab initio GW theory and angle-resolved photoemission spectroscopy, *Phys. Rev. B* **107**, 235107 (2023).
- [97] F. Moro, S. Ke, A. G. del Águila, A. Söll, Z. Sofer, Q. Wu, M. Yue, L. Li, X. Liu, and M. Fanciulli, Revealing 2D Magnetism in a Bulk CrSBr Single Crystal by Electron Spin Resonance, *Adv. Funct. Mater.* **32**, 2207044 (2022).

- [98] C. Boix-Constant, S. Mañas-Valero, A. M. Ruiz, A. Rybakov, K. A. Konieczny, S. Pillet, J. J. Baldoví, and E. Coronado, Probing the Spin Dimensionality in Single-Layer CrSBr Van Der Waals Heterostructures by Magneto-Transport Measurements, *Adv. Mater.* **34**, 2204940 (2022).
- [99] D. J. Rizzo et al., Visualizing Atomically Layered Magnetism in CrSBr, *Adv. Mater.* **34**, 2201000 (2022).
- [100] A. Scheie, M. Ziebel, D. G. Chica, Y. J. Bae, X. Wang, A. I. Kolesnikov, X. Zhu, and X. Roy, Spin Waves and Magnetic Exchange Hamiltonian in CrSBr, *Adv. Sci.* **9**, 2202467 (2022).
- [101] D. J. Newman and B. Ng, editors, *Crystal Field Handbook* (Cambridge University Press, Cambridge, UK ; New York, USA, 2000).
- [102] Y. Ahn, X. Guo, S. Son, Z. Sun, and L. Zhao, Progress and prospects in two-dimensional magnetism of van der Waals materials, *Prog. Quantum Electron.* **93**, 100498 (2024).
- [103] A. P. Cracknell, *Magnetism in Crystalline Materials: Applications of the Theory of Groups of Cambiant Symmetry*, 1. Aufl (Elsevier Reference Monographs, S.I., 2016).
- [104] O. Göser, W. Paul, and H. G. Kahle, Magnetic properties of CrSBr, *J. Magn. Magn. Mater.* **92**, 129 (1990).
- [105] A. Krimmel et al., Incommensurate structure of the spin-Peierls compound TiOCl in zero and finite magnetic fields, *Phys. Rev. B* **73**, 172413 (2006).
- [106] A. Schönleber, S. van Smaalen, and L. Palatinus, Structure of the incommensurate phase of the quantum magnet TiOCl, *Phys. Rev. B* **73**, 214410 (2006).
- [107] M. Shaz, S. van Smaalen, L. Palatinus, M. Hoinkis, M. Klemm, S. Horn, and R. Claessen, Spin-Peierls transition in TiOCl, *Phys. Rev. B* **71**, 100405 (2005).
- [108] A. Schönleber, J. Angelkort, S. van Smaalen, L. Palatinus, A. Senyshyn, and W. Morgenroth, Phase transition, crystal structure, and magnetic order in VOCl, *Phys. Rev. B* **80**, 064426 (2009).
- [109] A. Wiedenmann, J. P. Venien, P. Palvadeau, and J. Rossat-Mignod, Magnetic ordering of the quasi-two-dimensional system VOCl, *J. Phys. C Solid State Phys.* **16**, 5339 (1983).
- [110] J. Angelkort, A. Wölfel, A. Schönleber, S. van Smaalen, and R. K. Kremer, Observation of strong magnetoelastic coupling in a first-order phase transition of CrOCl, *Phys. Rev. B* **80**, 144416 (2009).
- [111] B. Das et al., Metamagnetism and Magnetocaloric Properties in a van der Waals Antiferromagnet CrOCl, *Phys. Status Solidi B* **260**, 2200422 (2023).
- [112] L. Yang, Y. Gong, Y. Lv, S. Huang, P. Huang, and D. Huo, Magnetic and thermodynamic study of the interplay between magnetism and structure in CrOCl, *J. Alloys Compd.* **982**, 173845 (2024).
- [113] M. Zhang et al., Spin-Lattice Coupled Metamagnetism in Frustrated van der Waals Magnet CrOCl, *Small* **19**, 2300964 (2023).
- [114] J. Zhang, A. Wölfel, L. Li, S. van Smaalen, H. L. Williamson, and R. K. Kremer, Magnetoelastic coupling in the incommensurate antiferromagnetic phase of FeOCl, *Phys. Rev. B* **86**, 134428 (2012).
- [115] J. Cenker et al., Reversible strain-induced magnetic phase transition in a van der Waals magnet, *Nat. Nanotechnol.* **17**, 256 (2022).
- [116] B. Xu, S. Li, K. Jiang, J. Yin, Z. Liu, Y. Cheng, and W. Zhong, Switching of the magnetic anisotropy via strain in two dimensional multiferroic materials: CrSX (X = Cl, Br, I), *Appl. Phys. Lett.* **116**, 052403 (2020).
- [117] K. Yang, G. Wang, L. Liu, D. Lu, and H. Wu, Triaxial magnetic anisotropy in the two-dimensional ferromagnetic semiconductor CrSBr, *Phys. Rev. B* **104**, 144416 (2021).
- [118] D. L. Esteras, A. Rybakov, A. M. Ruiz, and J. J. Baldoví, Magnon Straintronics in the 2D van der Waals Ferromagnet CrSBr from First-Principles, *Nano Lett.* **22**, 8771 (2022).
- [119] Y. Diao, C. Jin, X. Gu, Z. Lu, J. Zhang, Z. Dong, D. Liu, H. Fu, and C. Zhong, Strain-regulated magnetic phase transition and perpendicular magnetic anisotropy in CrSBr monolayer, *Phys. E Low-Dimens. Syst. Nanostructures* **147**, 115590 (2023).

- [120] C. Hou, X. Wang, Y. Sun, Y. Lu, and J. Ni, Magnetic–Electronic Coupling in the Strained Bilayer CrSBr, *J. Phys. Chem. C* **127**, 22833 (2023).
- [121] B. Wang, Y. Wu, Y. Bai, P. Shi, G. Zhang, Y. Zhang, and C. Liu, Origin and regulation of triaxial magnetic anisotropy in the ferromagnetic semiconductor CrSBr monolayer, *Nanoscale* **15**, 13402 (2023).
- [122] K. Bagani et al., Imaging Strain-Controlled Magnetic Reversal in Thin CrSBr, *Nano Lett.* **24**, 13068 (2024).
- [123] F. Fei, Y. Mao, W. Fang, W. Liu, J. P. Rollins, A. L. N. Kondusamy, B. Lv, Y. Ping, Y. Wang, and J. Xiao, Spin-Mechanical Coupling in 2D Antiferromagnet CrSBr, *Nano Lett.* **24**, 10467 (2024).
- [124] J. Klein et al., Control of structure and spin texture in the van der Waals layered magnet CrSBr, *Nat. Commun.* **13**, 5420 (2022).
- [125] S. van Smaalen, L. Palatinus, and A. Schönleber, Incommensurate interactions and nonconventional spin-Peierls transition in TiOBr, *Phys. Rev. B* **72**, 020105 (2005).
- [126] H. Schäfer, F. E. Wittig, and M. Jori, Untersuchungen am System $\text{Fe}_2\text{O}_3\text{-FeCl}_3\text{-H}_2\text{O-HCl}$. IX. Die thermochemische Beständigkeit des Eisenoxychlorids FeOCl, *Z. Für Anorg. Allg. Chem.* **287**, 61 (1956).
- [127] H. Schäfer and F. Wartenpfehl, Über das Vanadin(III)-oxydchlorid VOCl, *J. Common Met.* **3**, 29 (1961).
- [128] H. Schäfer and F. Wartenpfehl, Das Chrom (III)-oxydchlorid CrOCl, *Z. Für Anorg. Allg. Chem.* **308**, 282 (1961).
- [129] H. Schäfer, F. Wartenpfehl, and E. Weise, Über Titanchloride. V. Titan(III)-oxychlorid, *Z. Für Anorg. Allg. Chem.* **295**, 268 (1958).
- [130] S. M. Kauzlarich, J. L. Stanton, J. Faber, and B. A. Averill, Neutron profile refinement of the structure of FeOCl and $\text{FeOCl}(\text{TTF})_{1/8.5}$, *J. Am. Chem. Soc.* **108**, 7946 (1986).
- [131] A. Adam and G. Buisson, Structure magnétique cycloïdale de FeOCl, *Phys. Status Solidi A* **30**, 323 (1975).
- [132] A. Haase and G. Brauer, Vanadium oxychloride, *Acta Crystallogr. B* **31**, 2521 (1975).
- [133] S. R. Hwang, W.-H. Li, K. C. Lee, J. W. Lynn, and C.-G. Wu, Spiral magnetic structure of Fe in Van der Waals gapped FeOCl and polyaniline-intercalated FeOCl, *Phys. Rev. B* **62**, 14157 (2000).
- [134] A. Seidel, C. A. Marianetti, F. C. Chou, G. Ceder, and P. A. Lee, $S=1/2$ chains and spin-Peierls transition in TiOCl, *Phys. Rev. B* **67**, 020405 (2003).
- [135] A. C. Komarek, T. Taetz, M. T. Fernández-Díaz, D. M. Trots, A. Möller, and M. Braden, Strong magnetoelastic coupling in VOCl: Neutron and synchrotron powder x-ray diffraction study, *Phys. Rev. B* **79**, 104425 (2009).
- [136] T. Zhang et al., Magnetism and Optical Anisotropy in van der Waals Antiferromagnetic Insulator CrOCl, *ACS Nano* **13**, 11353 (2019).
- [137] K. Yang et al., Unconventional correlated insulator in CrOCl-interfaced Bernal bilayer graphene, *Nat. Commun.* **14**, 2136 (2023).
- [138] R. J. Beynon and J. A. Wilson, TiOCl, TiOBr—are these RVB $d1$, $S=1/2$ materials? The results of scandium substitution set in the context of other $S=1/2$ systems of current interest for high-temperature superconductivity and the metal-insulator transition, *J. Phys. Condens. Matter* **5**, 1983 (1993).
- [139] T. Sasaki, M. Mizumaki, K. Kato, Y. Watabe, Y. Nishihata, M. Takata, and J. Akimitsu, Observation of Phase Transition with Lattice Distortion in the Low-dimensional Quantum Spin System TiOBr by Synchrotron X-ray Diffraction –Evidence of Spin-Peierls Transition?–, *J. Phys. Soc. Jpn.* **74**, 2185 (2005).
- [140] F. Marques-Moros, C. Boix-Constant, S. Mañas-Valero, J. Canet-Ferrer, and E. Coronado, Interplay between Optical Emission and Magnetism in the van der Waals Magnetic Semiconductor CrSBr in the Two-Dimensional Limit, *ACS Nano* **17**, 13224 (2023).

- [141] Y. J. Bae et al., Exciton-coupled coherent magnons in a 2D semiconductor, *Nature* **609**, 282 (2022).
- [142] G. M. Diederich et al., Tunable interaction between excitons and hybridized magnons in a layered semiconductor, *Nat. Nanotechnol.* **18**, 23 (2022).
- [143] W. M. Linhart, M. Rybak, M. Birowska, P. Scharoch, K. Mosina, V. Mazanek, D. Kaczorowski, Z. Sofer, and R. Kudrawiec, Optical markers of magnetic phase transition in CrSBr, *J. Mater. Chem. C* **11**, 8423 (2023).
- [144] K. Lin et al., Strong Exciton–Phonon Coupling as a Fingerprint of Magnetic Ordering in van der Waals Layered CrSBr, *ACS Nano* **18**, 2898 (2024).
- [145] A. Pawbake et al., Magneto-Optical Sensing of the Pressure Driven Magnetic Ground States in Bulk CrSBr, *Nano Lett.* **23**, 9587 (2023).
- [146] E. J. Telford et al., Designing Magnetic Properties in CrSBr through Hydrostatic Pressure and Ligand Substitution, *Adv. Phys. Res.* **2**, 2300036 (2023).
- [147] F. Tabataba-Vakili et al., Doping-control of excitons and magnetism in few-layer CrSBr, *Nat. Commun.* **15**, 4735 (2024).
- [148] K. Xie, X.-W. Zhang, D. Xiao, and T. Cao, Engineering Magnetic Phases of Layered Antiferromagnets by Interfacial Charge Transfer, *ACS Nano* **17**, 22684 (2023).
- [149] J. Jo, S. Mañas-Valero, E. Coronado, F. Casanova, M. Gobbi, and L. E. Hueso, Nonvolatile Electric Control of Antiferromagnet CrSBr, *Nano Lett.* **24**, 4471 (2024).
- [150] C. Boix-Constant, S. Jenkins, R. Rama-Eiroa, E. J. G. Santos, S. Mañas-Valero, and E. Coronado, Multistep magnetization switching in orthogonally twisted ferromagnetic monolayers, *Nat. Mater.* **23**, 212 (2023).
- [151] Y. Chen, K. Samanta, N. A. Shahed, H. Zhang, C. Fang, A. Ernst, E. Y. Tsybal, and S. S. P. Parkin, Twist-assisted all-antiferromagnetic tunnel junction in the atomic limit, *Nature* **632**, 1045 (2024).
- [152] J. Liu, X. Zhang, and G. Lu, Moiré magnetism and moiré excitons in twisted CrSBr bilayers, *Proc. Natl. Acad. Sci.* **122**, e2413326121 (2025).
- [153] M. L. Feuer et al., *Doping-Induced Charge Density Wave and Ferromagnetism in the Van Der Waals Semiconductor CrSBr*, arXiv:2412.08631.
- [154] K. Mosina, B. Wu, N. Antonatos, J. Luxa, V. Mazánek, A. Söll, D. Sedmidubsky, J. Klein, F. M. Ross, and Z. Sofer, Electrochemical Intercalation and Exfoliation of CrSBr into Ferromagnetic Fibers and Nanoribbons, *Small Methods* **8**, 2300609 (2024).
- [155] F. Long et al., Ferromagnetic Interlayer Coupling in CrSBr Crystals Irradiated by Ions, *Nano Lett.* **23**, 8468 (2023).
- [156] K. Torres, A. Kuc, L. Maschio, T. Pham, K. Reidy, L. Dekanovsky, Z. Sofer, F. M. Ross, and J. Klein, Probing Defects and Spin-Phonon Coupling in CrSBr via Resonant Raman Scattering, *Adv. Funct. Mater.* **33**, 2211366 (2023).
- [157] K. Lin et al., Probing the Band Splitting near the Γ Point in the van der Waals Magnetic Semiconductor CrSBr, *J. Phys. Chem. Lett.* **15**, 6010 (2024).
- [158] C. Meineke et al., Ultrafast Exciton Dynamics in the Atomically Thin van der Waals Magnet CrSBr, *Nano Lett.* **24**, 4101 (2024).
- [159] J. Klein et al., Sensing the local magnetic environment through optically active defects in a layered magnetic semiconductor, *ACS Nano* **17**, 288 (2023).
- [160] Y. J. Bae et al., Transient magnetoelastic coupling in CrSBr, *Phys. Rev. B* **109**, 104401 (2024).
- [161] Y. Sun, F. Meng, C. Lee, A. Soll, H. Zhang, R. Ramesh, J. Yao, Z. Sofer, and J. Orenstein, Dipolar spin wave packet transport in a van der Waals antiferromagnet, *Nat. Phys.* **20**, 794 (2024).
- [162] T. M. J. Cham, S. Karimeddiny, A. H. Dismukes, X. Roy, D. C. Ralph, and Y. K. Luo, Anisotropic Gigahertz Antiferromagnetic Resonances of the Easy-Axis van der Waals Antiferromagnet CrSBr, *Nano Lett.* **22**, 6716 (2022).
- [163] A. N. Christensen, T. Johansson, and S. Quézel, Preparation and Magnetic Properties of CrOCl., *Acta Chem. Scand.* **28a**, 1171 (1974).

- [164] J. Cenker et al., *Strain-Programmable van Der Waals Magnetic Tunnel Junctions*, arXiv:2301.03759.
- [165] Y. Cao et al., Correlated insulator behaviour at half-filling in magic-angle graphene superlattices, *Nature* **556**, 80 (2018).
- [166] C. Jin et al., Observation of moiré excitons in WSe₂/WS₂ heterostructure superlattices, *Nature* **567**, 76 (2019).
- [167] L. Wang et al., Correlated electronic phases in twisted bilayer transition metal dichalcogenides, *Nat. Mater.* **19**, 861 (2020).
- [168] P. Wang et al., One-dimensional Luttinger liquids in a two-dimensional moiré lattice, *Nature* **605**, 57 (2022).
- [169] T. Song et al., Direct visualization of magnetic domains and moiré magnetism in twisted 2D magnets, *Science* **374**, 1140 (2021).
- [170] H. Xie et al., Twist engineering of the two-dimensional magnetism in double bilayer chromium triiodide homostructures, *Nat. Phys.* **18**, 30 (2022).
- [171] Y. Xu et al., Coexisting ferromagnetic–antiferromagnetic state in twisted bilayer CrI₃, *Nat. Nanotechnol.* **17**, 143 (2022).
- [172] H. Xie et al., Evidence of non-collinear spin texture in magnetic moiré superlattices, *Nat. Phys.* **19**, 1150 (2023).
- [173] Z. Zhai, W. Liu, X. Guo, L. Zhao, and B. Lv, *Engineering Magnetism and Electronic Behavior of Bulk CrSBr via Electrochemical Intercalation*, (unpublished).
- [174] S. Jiang, J. Shan, and K. F. Mak, Electric-field switching of two-dimensional van der Waals magnets, *Nat. Mater.* **17**, 406 (2018).
- [175] B. Huang et al., Electrical control of 2D magnetism in bilayer CrI₃, *Nat. Nanotechnol.* **13**, 544 (2018).
- [176] J. Yu et al., Direct Imaging of Antiferromagnet-Ferromagnet Phase Transition in van der Waals Antiferromagnet CrSBr, *Adv. Funct. Mater.* **34**, 2307259 (2024).
- [177] Z. Sun et al., Resolving and routing magnetic polymorphs in a 2D layered antiferromagnet, *Nat. Mater.* **24**, 226 (2025).
- [178] W. Liu and B. Lv, *Quantum-Spin-Liquid-Like State with Charge Neutron Fermions in a New Triangular Lattice of Cr-Se-Br*, (unpublished).
- [179] V. Krämer, Structure of the bismuth chloride sulphide Bi₄Cl₂S₅, *Acta Crystallogr. B* **35**, 139 (1979).
- [180] H. Oppermann, Untersuchungen an Vanadinoxidchloriden und Vanadinchloriden. I. Gleichgewichte mit VOCl₃, VO₂Cl und VOCl₂, *Z. Für Anorg. Allg. Chem.* **351**, 113 (1967).
- [181] A. Ghosh et al., Magnetic circular dichroism in the dd excitation in the van der Waals magnet CrI₃ probed by resonant inelastic x-ray scattering, *Phys. Rev. B* **107**, 115148 (2023).
- [182] M. A. Tschudin et al., Imaging nanomagnetism and magnetic phase transitions in atomically thin CrSBr, *Nat. Commun.* **15**, 6005 (2024).
- [183] T. S. Ghiasi, M. Borst, S. Kurdi, B. G. Simon, I. Bertelli, C. Boix-Constant, S. Mañas-Valero, H. S. J. van der Zant, and T. van der Sar, Nitrogen-vacancy magnetometry of CrSBr by diamond membrane transfer, *Npj 2D Mater. Appl.* **7**, 1 (2023).
- [184] M.-P. Miao, N. Liu, W.-H. Zhang, D.-B. Wang, W. Ji, and Y.-S. Fu, *Spin-Resolved Imaging of Atomic-Scale Helimagnetism in Monolayer NiI₂*, arXiv:2309.16526.
- [185] A. Chakraborty et al., Magnetic Skyrmions in a Thickness Tunable 2D Ferromagnet from a Defect Driven Dzyaloshinskii–Moriya Interaction, *Adv. Mater.* **34**, 2108637 (2022).
- [186] T. S. Ghiasi, A. A. Kaverzin, A. H. Dismukes, D. K. de Wal, X. Roy, and B. J. van Wees, Electrical and thermal generation of spin currents by magnetic bilayer graphene, *Nat. Nanotechnol.* **16**, 788 (2021).
- [187] A. A. Kaverzin, T. S. Ghiasi, A. H. Dismukes, X. Roy, and B. J. van Wees, Spin injection by spin-charge coupling in proximity induced magnetic graphene, *2D Mater.* **9**, 045003 (2022).

- [188] A. Söll et al., High- κ Wide-Gap Layered Dielectric for Two-Dimensional van der Waals Heterostructures, *ACS Nano* **18**, 10397 (2024).
- [189] L. Li et al., Ultrathin Van der Waals Lanthanum Oxychloride Dielectric for 2D Field-Effect Transistors, *Adv. Mater.* 2309296 (n.d.).
- [190] W. Zeng, J. Li, L. Feng, H. Pan, X. Zhang, H. Sun, and Z. Liu, Synthesis of Large-Area Atomically Thin BiOI Crystals with Highly Sensitive and Controllable Photodetection, *Adv. Funct. Mater.* **29**, 1900129 (2019).